Electrochimica Acta 296 (2019) 676–682

Contents lists available at ScienceDirect

Electrochimica Acta

journal homepage: www.elsevier.com/locate/electacta

# Improved high-rate performance of a supercapacitor electrode from manganese-oxide-coated vertically aligned carbon nanotubes prepared by a pulsed current electrodeposition method

Meng Li, Hyung Gyu Park*, [1]

*Eidgenössische Technische Hochschule (ETH) Zürich, Zürich CH-8092, Switzerland*

ARTICLE INFO

*Article history:*
Received 11 August 2018
Received in revised form
26 October 2018
Accepted 10 November 2018
Available online 15 November 2018

*Keywords:*
Supercapacitor
High-rate performance
Vertically aligned carbon nanotube
Manganese oxide
Pulsed current electrodeposition

ABSTRACT

Although manganese oxide ($MnO_2$) can be incorporated with vertically aligned carbon nanotubes (VACNTs) to improve supercapacitor performance potentially, one of the hurdles that hampers this embodiment is a difficulty of coating $MnO_2$ on VACNTs homogeneously. As a way of overcoming this hurdle, we present here a facile method of pulsed current electrodeposition that turns out to exceed conventional methods in coating quality. Such improvement leads to a clear enhancement in gravimetric specific capacitance, reaching a state-of-the-art value of 243.3 F/g at a high scanning rate of 100 mV/s. In the course of this characterization, diffusion hindrance through a $MnO_2$ layer clogging over VACNTs is found out to limit the device performance at high mass loading. An empirical relationship is proposed to explain such phenomenon and demonstrates good application in various conditions. The optimized VACNTs/$MnO_2$ electrode also reveals outstanding high-rate performances.



## 1. Introduction

Increasing demand of clean and renewable energy has set up a request for electrochemical storage. Though being able to operate rapidly, conventional double-layer-based supercapacitors (SCs) alone cannot often store sufficient energy [1]. Pseudocapacitive materials are considered to hold promise in boosting the SC energy density, approaching that of batteries [2]. Thanks to the high theoretical specific capacitance ($C_m$), environmental friendliness, rich earth abundance, and modest material cost, manganese oxide ($MnO_2$) has been drawing great attentions for use in SC electrodes [3,4]. Nevertheless, its poor conductivity ($10^{-6}$–$10^{-5}$ S/cm) remains a major obstacle that thwarts utilization of its full potential particularly in high-rate operation [3]. It has also been revealed that the increased resistance can severely deteriorate the performance of thickly $MnO_2$-coated SC electrodes [5].

A practical strategy is to develop a composite electrode in which $MnO_2$ is effectively dispersed into other highly porous and conductive materials, such as nanoporous metal [6], activated carbon [7–9], graphene [10–13], and carbon nanotube (CNT) [5,14–33]. Compared with other scaffold materials, vertically aligned CNTs (VACNTs) are of particular interest, as they provide a lightweight, binder-free, and low-resistance platform that could be potentially scaled up in mass loading without sacrificing coating effectiveness [34]. The unique structure of VACNTs also makes it especially useful as vertical interconnect [35] in integrated circuits, which is compatible for on-chip supercapacitor application [36]. Additionally, since $\alpha$-$MnO_2$ possesses similar conduction band minimal energy (4.9 eV) [37] to the work function of CNTs (4.8–4.9 eV) [38], electrons can be injected from $MnO_2$ into CNT in a nearly barrier-less manner. A thin layer of $MnO_2$ that coats individual nanotubes of VACNTs homogeneously can thus allow facile transport of electrons, rather than taking the scattering pathways between adjacent $MnO_2$ particles or within a $MnO_2$ layer. The optimal coating thickness (or mass) of $MnO_2$ in such rational design, nevertheless, remains unknown. $MnO_2$ could be electrodeposited using anodic oxidation of $Mn^{2+}$ either potentialstatically (at constant voltage ramp rate) or galvanostatically (at constant direct current), yet showing very similar $C_m$ [39]. More details in electrodeposited $MnO_2$ for supercapacitor applications can be found in literature [2,40]. To coat $MnO_2$ on non-aligned CNTs, direct current electrodeposition (DCE) is favored for its good controllability [14–19]. When it comes to VACNTs, however, diffusion

* Corresponding author.
*E-mail addresses:* parkh@ethz.ch, parkhg@postech.ac.kr (H.G. Park).
[1] Mechanical Engineering, Pohang University of Science and Technology (POSTECH), 77 Cheongam-ro, Nam-gu, Pohang, Gyeongbuk, Republic of Korea.

https://doi.org/10.1016/j.electacta.2018.11.062
0013-4686/

hindrance prevents precursor molecules from penetrating into the CNT forest deeply such that $MnO_2$ tends to clog over VACNTs instead of coating each CNT conformally [20,21]. The resulting electrode naturally suffers from poor performance caused by the non-ideal coating quality.

To resolve these issues, here we employ pulsed current deposition (PCE), a technique that have already been found instrumental to improve coating quality on an isolated CNT [41,42] or CNT mesh [14,29] but seldom on VACNTs [24]. We demonstrate that the PCE method can improve $MnO_2$ coating conformity by balancing the precursor ionic diffusion within the CNT forest. Consequently, the increased effectiveness of the pseudocapacitive layer renders the optimized composite electrode an unprecedentedly large specific capacitance particularly at high rate.

## 2. Experimental

### 2.1. Material synthesis

20-nm-thick Al and 3-nm-thick Fe were deposited via e-beam evaporation on 1 cm × 1 cm Ni foils (Alfa Aesar, 99% metal basis, 0.025 mm in thickness) as catalyst. CNT growth using chemical vapor deposition (CVD) was then carried out in a hot-wall quartz-tube furnace (Lindberg Blue M™ Mini-Mite™) at atmosphere pressure. Ni foils were loaded into the quartz tube and heated up to 750 °C at 30 °C/min, with 600 sccm of $H_2$ and 400 sccm of Ar flow rates. After annealing at this temperature for 20 min, additional $C_2H_4$ (250 sccm) was introduced to the furnace to initiate the VACNT growth with varying the nanotube height, or the VACNT mass. Upon completion of the growth step, the reactor was cooled in Ar atmosphere to room temperature. The mass of VACNT was determined by weighing it with a high-precision analytical microbalance (Mettler Toledo, XPE 105) before and after the growth. For simplicity, samples were named after their growth time, *i.e.*, 1-min-VACNTs, 3-min-VACNTs and 10-min-VACNTs. Typical growth rate was ~10 μm/min in terms of the forest thickness of or equivalently ~20 μg/min in terms of the mass of VACNT.

Electrodeposition of $MnO_2$ was carried out using a three-electrode configuration in an electrochemical workstation (CH Instrument, CHI 660E). The VACNT-coated Ni foil was connected electrically to a Cu tape at the backside to external circuit and then encapsulated with an insulating polyimide (Kapton) tape, exposing approximately 0.8 cm × 0.8 cm of effective area for a working electrode. A Pt wire was used as counter electrode, and a standard Ag/AgCl as a reference electrode. The solution for deposition was an aqueous mixture of 0.1 M $Na_2SO_4$ and 0.02 M $MnSO_4$. Three different pulse widths (a 100% duty cycle in DCE with $t_{off} = 0$ ms, a 50% duty cycle with $t_{on} = t_{off} = 5$ ms in PCE 50%, and a 10% duty cycle with $t_{on} = 5$ ms and $t_{off} = 45$ ms in PCE 10%) were tested to optimize the electrodeposition condition. A deposition current of 5 mA was chosen particularly to ensure a high nucleation density without anodic oxygen evolution. For quick assessment, the mass of deposited $MnO_2$ was estimated from Faraday's law of electrolysis assuming 100% current efficiency. To obtain a better accuracy, the working electrode was thoroughly cleaned with deionized water and vacuum dried at 50 °C for 2 h before weighed.

### 2.2. Electrochemical and material characterization

Electrochemical measurements were conducted using the same setup except that the electrolyte was replaced by a $Na_2SO_4$ aqueous solution (1 M). Cyclic voltammetry (CV) scanning was performed in a potential range ($V_t$) from 0 V to 0.8 V at various scanning rates ($v$). Total capacitance of the electrode ($C_{total}$), is calculated from eq. (1), in which $I$ is the current.

$$C_{total} = \frac{\int IdV}{2V_t v} \tag{1}$$

Gravimetric specific capacitance ($C_m$) of the electrode is then defined by dividing the total mass $m$, which consists $m_{CNT}$ *and* $m_{MnO2}$ as the mass of VACNT matrix and $MnO_2$ loading, respectively. Areal specific capacitance ($C_a$) is calculated by normalizing to the working electrode area ($A$).

$$C_m = \frac{C_{total}}{m_{CNT} + m_{MnO_2}} \tag{2}$$

$$C_a = \frac{C_{total}}{A} \tag{3}$$

Galvanostatic charging and discharging (GCD) measurement was done in the same potential window but at different currents. $C_m$ could also be obtained from eq. (4) during a discharging process after initial IR drop ($V_{IR}$).

$$C_m = \frac{2I\int_{t_c}^{t_c+t_d} Vdt}{m(V_t - V_{IR})^2} \tag{4}$$

In this equation $t_c$ and $t_d$ are charging and discharging time, respectively, and thus Coulombic efficiency $\eta$ is defined as:

$$\eta = \frac{t_d}{t_c} \tag{5}$$

Electrochemical impedance (EIS) was measured at a working-counter electrode distance of ~4 cm and at frequency ranging from 0.1 Hz to 100 kHz at open circuit potential with an alternating amplitude of 5 mV.

Structure and morphology of the working electrode were characterized using scanning electron microscope (SEM, Hitachi, SU 8230). Quality of VACNTs and phase information of as-deposited $MnO_2$ were determined using a Raman spectroscope (Renishaw inVia™) at 785 nm of an incident laser wavelength at 1% of the laser power. X-ray diffraction (XRD) spectrum of the sample was obtained with an X-ray diffractometer (Bruker, D8 Discover) using Cu Kα radiation source (0.15418 nm in wavelength).

## 3. Results and discussion

Scanning electron micrographs of 10-min-VACNT/$MnO_2$ samples reveal that at ~230 μg of $MnO_2$ mass loading ($m_{MnO2}$) prepared via DCE, the top of the VACNT matrix is almost fully covered with granular $MnO_2$ (~1 μm in size) (Fig. 1a). As proposed by a previous report [21], this clogging layer will block additional entrance of $Mn^{2+}$ inside the CNT forest, leading to concentration drop and very little amount of coating near the bottom end (Fig. 1e). For samples prepared via PCE, on the other hand, $MnO_2$ growth pauses during a resting period ($t_{off}$). With the same amount of deposition, smaller granules are formed (~500 nm in size) atop VACNTs, possibly leaving more (and larger) diffusion pathways. Moreover, $Mn^{2+}$ ions can penetrate the CNT forest during the resting period, balancing the concentration polarization. As a result, more material is able to coat around CNTs (Fig. 1d, f), resulting in better coating quality. However, even with PCE, an obvious clogging layer still forms near the top few microns of the CNT forest at very high $m_{MnO2}$. With time, it is noticed that $MnO_2$ grows into granules (Figs. S2a–d), which eventually overlap with one another and almost fully block the top of VACNTs. A gradual decrease in the granule size is also observed from top to bottom (Fig. 1d), suggesting non-conformal

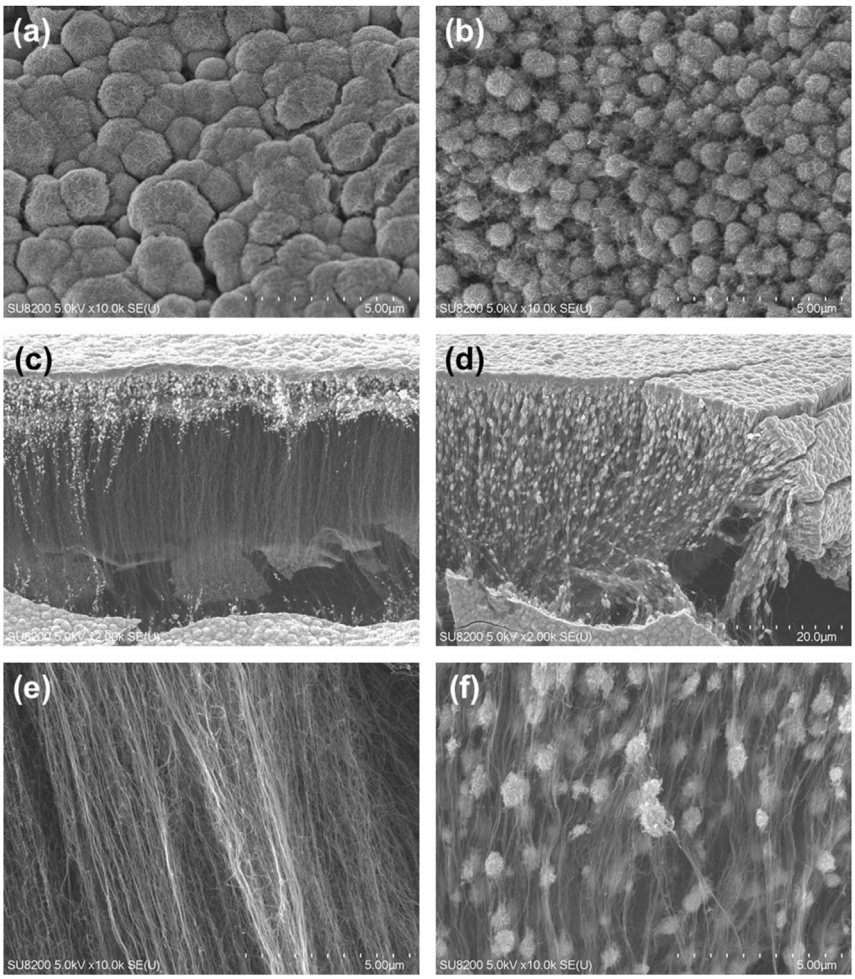


**Fig. 1.** (a, b) Top-view SEM images of 10-min-VACNTs/$MnO_2$ samples prepared by DCE (a) and PCE 10% (b), at ~230 μg mass loading. (c, d) Cross-section-view of the samples prepared by DCE (c) and PCE 10% (d), at ~575 μg mass loading. (e, f) Magnified view of (c) and (d) near the bottom end, respectively.

coating. The latter problem can be mitigated by switching to a shorter matrix (1-min-VACNTs, for example) with decreased ion diffusion lengths. In this way, $MnO_2$ granules can be formed into a nearly uniform size (~300 nm) along nanotubes (Fig. S2f).

To fabricate an effective SC electrode, it is of great importance to optimize $C_m$. SEM study expresses that too much deposition may only sacrifice device performance and waste material. To locate the optimal $m_{MnO2}$, a series of cyclic voltammetry (CV) experiments were performed. Fig. 2a shows typical CV scanning of a 10-min-VACNTs/$MnO_2$ sample prepared using PCE 10% (see the rest CV curves in Fig. S1). When pseudocapacitive $MnO_2$ is added to VACNTs, $C_m$, which is proportional to the area circled by the CV curve, rises monotonically with $m_{MnO2}$ and saturates at ~235.2 μg. At the same time, the curve becomes distorted, behaving more "resistor-like" due to the increased thickness of $MnO_2$ coating. The Faradaic peaks (pointed by the arrow), originated from the intercalation (and deintercalation) of $Na^+$ into $MnO_2$ [43–45], tend to shift outside the voltage window. When $m_{MnO2}$ becomes too large, the incomplete Faradaic reaction likely weakens the trend of increasing in $C_m$.

We calculate $C_m$ versus $m_{MnO2}$ in Fig. 2c. For a sample prepared via DCE, the maximum value of $C_m$ is found to be 101.7 F/g at mass loading of 311.3 μg. By introducing $t_{off}$ (5 ms in PCE 50%) during deposition, maximum $C_m$ upgrades to 128.9 F/g. Prolonging $t_{off}$ to 45 ms (PCE 10%) leads to further improvement up to 138.9 F/g. This finding matches with the improved coating quality (Fig. 1). Additionally, when shorter VACNTs are used, maximum $C_m$ can be further increased; for 3-min- and 1-min-VACNTs/$MnO_2$ samples, maximum $C_m$ values are obtained at 198.8 F/g and 243.3 F/g with corresponding $m_{MnO2}$ dropping to ~154.5 μg and ~50.7 μg, respectively. To make a fair comparison with reported $MnO_2$ based binary SC electrodes in aqueous electrolyte, $C_m$ values at a fast scanning rate of 100 mV/s are listed in Table 1. It should be noted that some literatures report $C_m$ by normalizing it to $m_{MnO2}$ rather than the total mass ($m_{total}$). Such a metric might be misleading if "non-active" mass (mass of CNT matrix, binder, and possibly the current collector in case a 3-dimensional metal foam is involved) takes up a significant portion of $m_{total}$. According to the tabulated values with correction to the best of our knowledge, $C_m$ of our optimized electrodes exceeds the literature record [19] by ~21.6%. In terms of areal specific capacitance ($C_a$), high-mass-loading electrodes (>20 mg/$cm^2$) [8,31] provide much larger values than ours, despite that the corresponding $C_m$ are smaller. This suggests that the material effectiveness in these electrodes is low.

Raman spectra confirms that crystalline phase of the as-deposited $MnO_2$ remains unchanged with the deposition condition (Fig. 2b). Therefore, better coating morphology, rather than phase, turns out to be responsible for the significant increase in $C_m$. In the two VACNTs/$MnO_2$ samples, peaks around 574 $cm^{-1}$ and 646 $cm^{-1}$ agree nearly perfectly with the literature value of $Na^+$

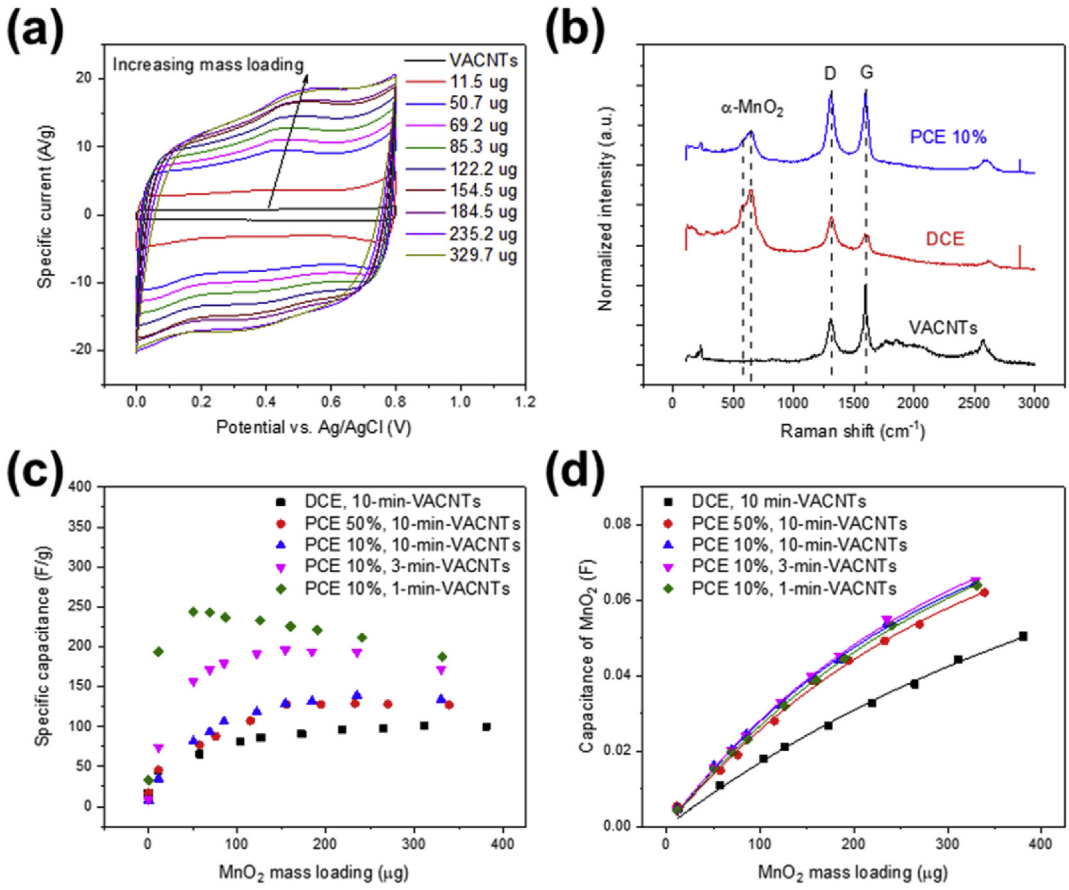


**Fig. 2.** (a) Cyclic voltammetry of PCE 10% deposited 10-min-VACNTs/$MnO_2$ sample at 100 mV/s with respect to different $MnO_2$ mass loading, (c) dependence of $MnO_2$ mass loading on the gravimetric specific capacitance, and (d) capacitance of $MnO_2$ for various VACNTs/$MnO_2$ SC electrodes, with fitting using eq. (6). (b) Raman spectra of 10-min-VACNTs and 10-min-VACNTs/$MnO_2$ samples coated with either DCE or PCE 10%. Mass loading of these two samples are similar.

**Table 1**
Summary of specific capacitance at 100 mV/s of $MnO_2$ based binary supercapacitor electrodes using flat current collectors. Abbreviations: SCE, saturated calomel electrode; AC, activated carbon; Gr, graphene.

| Reference | $C_m$ (F/g) | Voltage range | Preparation method | $C_a$ (mF/cm$^2$) |
|---|---|---|---|---|
| [5] | 50 | 0.1–0.8 V vs. Ag/AgCl | $MnO_2$ nanoflake and CNT co-filtration | 50 |
| [14] | 77 | −0.1–0.9 V vs. SCE | Voltage pulse deposition in CNT mesh | 47 |
| [19] | 200 | −0.1–0.8 V vs. SCE | DCE in CNT mesh with Gr additive | – |
| [21] | 179 | 0–1 V vs. SCE | $KMnO_4$ dropwise dipping in VACNTs | – |
| [27] | 100 | −0.1–0.9 V vs. SCE | $KMnO_4$ and $Mn^{2+}$ reaction with CNT | – |
| [29] | 75 | 0–0.8 V vs. Ag/AgCl | High voltage pulse deposition in CNT mesh | 200 |
| [31] | 10 | 0–0.9 V vs. SCE | $MnO_2$ CNT mixture at high loading | 700 |
| This work | 243.3 | 0–0.8 V vs. Ag/AgCl | PCE 10% on 1-min-VACNTs | 26.5 |
| [8] | 15 | −0.3–0.6 V vs. Ag/AgCl | Potenialstatic deposition on AC | 420 |
| [12] | 90 | −0.4–0.6 V vs. Ag/AgCl | $MnO_2$ nanorods mixed with Gr nanoflakes | – |

intercalated α-$MnO_2$ [46]. The α phase is considered preferable for the SC application given its large crystalline vacancies for cation intercalation [47]. D peak (1308 cm$^{-1}$) and G peak (1594 cm$^{-1}$) of VACNTs are determined according to the literature [48], and their intensity ratio ($I_D/I_G$) is calculated as 0.59 for as-grown VACNTs on a Ni foil. In a sample prepared via PCE and DCE, $I_D/I_G$ rises to 0.98 and 1.54, respectively, indicating more defects and increased resistivity [49]. The relative intensity of $MnO_2$ observed particularly pronounced for the DCE sample (Fig. 2b) is likely attributed to a clogging layer of $MnO_2$ on top of VACNTs, in agreement with the SEM images (Fig. 1a, c). X-ray diffraction spectrum also suggests the α phase of as-deposited $MnO_2$ (Fig. S3).

To explore the nature of capacitance of $MnO_2$ ($C_{MnO2}$), we extract it by deducting the capacitance of raw VACNTs ($C_{CNT}$) from $C_{total}$. Unlike a literature [42] in which the authors have managed to deposit $MnO_2$ electrochemically on an isolated CNT and observed a linear relationship between $C_{MnO2}$ and $m_{MnO2}$, we discover a nonlinear relationship in the case of $MnO_2$ coating on VACNTs (Fig. 2d). An empirical formula (eq. (6)) is proposed to fit this relationship nicely:

$$C_{MnO_2} = C_0\left(1 - \exp\left[-\frac{m_{MnO_2}}{m_0}\right]\right), \quad (6)$$

**Table 2**
Summary of fitting parameters used in eq. (6) for VACNTs/$MnO_2$ samples.

| VACNT growth time | Preparation method | $C_0$ (F) | $m_0$ (μg) | $C_0/m_0$ (F/g) |
|---|---|---|---|---|
| 10 min | DCE | 0.09695 | 522.6 | 185.5 |
| 10 min | PCE 50% | 0.09475 | 317.8 | 298.1 |
| 10 min | PCE 10% | 0.09437 | 286.7 | 329.2 |
| 3 min | PCE 10% | 0.09804 | 296.4 | 330.8 |
| 1 min | PCE 10% | 0.09993 | 322.5 | 309.9 |

$$C_{m,MnO_2} = \frac{dC_{MnO_2}}{dm_{MnO_2}} = \frac{C_0}{m_0}\exp\left[-\frac{m_{MnO_2}}{m_0}\right], \quad (7)$$

where $C_0$ represents the saturation capacitance, and $m_0$ is a fitting parameter related to the coating quality (see discussion below), values of which are tabulated (Table 2) for all the VACNT/$MnO_2$ samples characterized. A suitable description for the specific capacitance of $MnO_2$ ($C_{m,MnO2}$) can be given by the derivative of $C_{MnO2}$ with respect to $m_{MnO2}$ (eq. (7)). It predicts that high $m_{MnO2}$ decreases the effectiveness of $C_{m,MnO2}$, partly supported by $MnO_2$ clogging of VACNTs upon excessive $m_{MnO2}$ supply (Figs. S2a–c). As sizes of the diffusion pathway shrink with $MnO_2$ coating thickness, diffusion of the precursor ions apparently drops [50], thwarting further coating of $MnO_2$ inside the CNT forest. The process is analogous to membrane fouling [51] except that the pore blocking granules may grow. Supported in part by the SEM images of Fig. 1, a large $m_0$ value in the via-DCE-prepared sample implies that pore blockade could happen faster and more easily. A detailed mechanistic understanding associated with eq. (6) calls for further investigation.

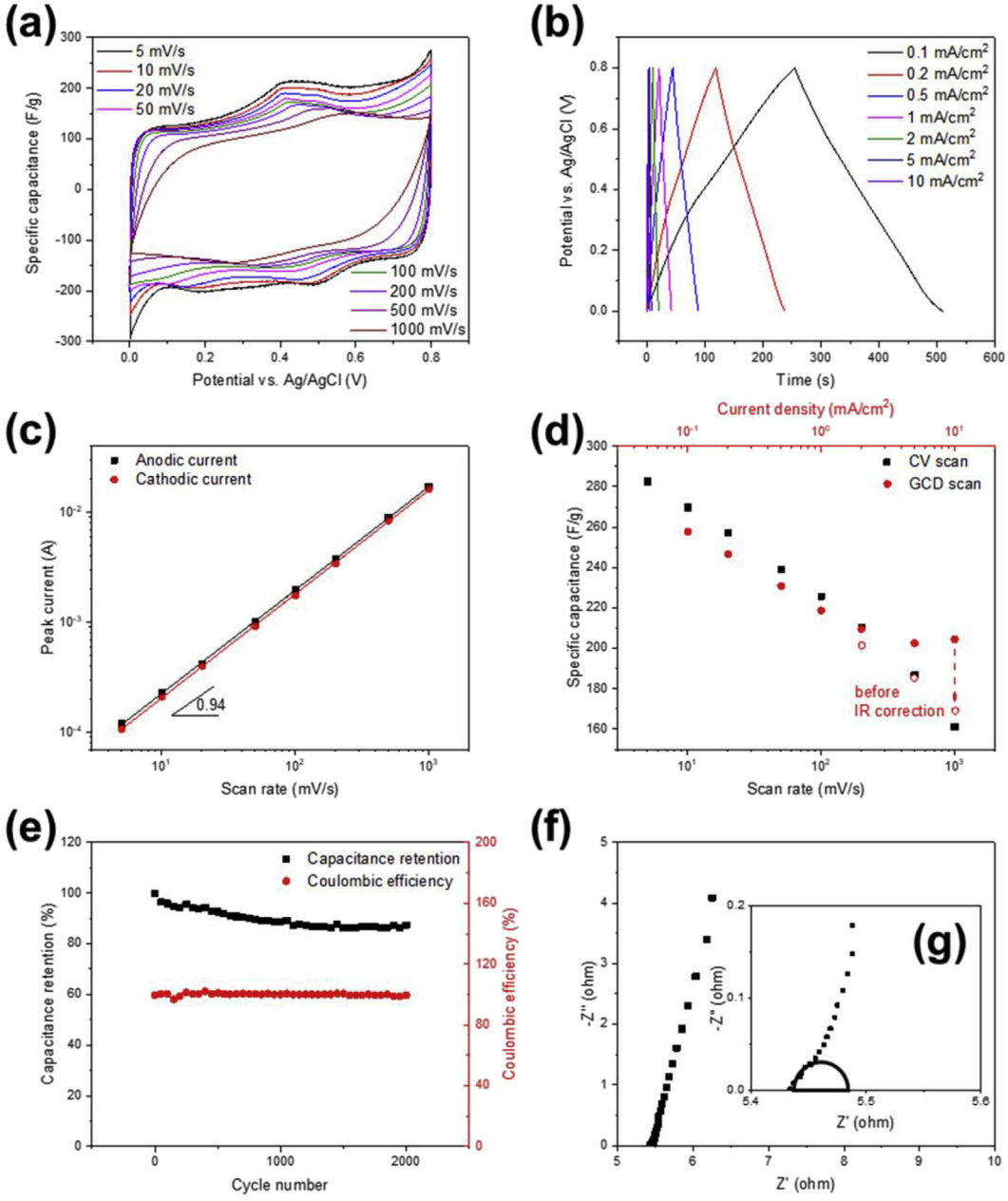


**Fig. 3.** Cyclic voltammetry (a), Galvanostatic charging and discharging spectra (b), peak current (c) and gravimetric specific capacitance (d) of a 1-min-VACNTs/50.7 μg $MnO_2$ sample prepared with PCE 10% in various scanning conditions. (e) Lifetime performance at 1 mA/cm² and (f) Nyquist plot with zoom-in view near horizontal axis (g) inset.

Similar values of $C_0$ are found for all samples, hinting the same mechanism of hindrance. Particularly, $C_{MnO2}$ of three PCE-10% samples nearly overlap with one another (Fig. 2d). The improvement of $C_m$ for short VACNTs, therefore, largely comes from the use of light matrices. Additionally, at very small amount of deposition (setting $m_{MnO2} = 0$ in eq. (7)), one can obtain the ultimate $C_{m,MnO2}$ as $C_0/m_0$, a value that is ideally unrestricted by hindered diffusion. For the 10-min-VACNT samples, the increasing trend of $C_0/m_0$ with respect to $t_{off}$ clearly conveys that the via-PCE-prepared samples have better (more homogeneous) coating quality, outperforming the via-DCE-prepared sample in terms of $C_{m,MnO2}$. When the same PCE 10% method was applied on VACNTs in different lengths, interestingly, $C_0/m_0$ remains more or less unchanged, showing a clogging-independent $C_{m,MnO2}$ at ~310–330 F/g. It is noteworthy that our result closely matches with the value obtained from thin $MnO_2$ coating on an isolated CNT (310 F/g at 15 mV/s) [42]. Even with limitations at high mass loading, this result bolsters the potential of PCE in rendering high-quality coating into the indentations of a very high aspect ratio.

Noticeably, less amount of $m_{MnO2}$ is needed to optimize lighter VACNTs. As $C_{CNT}$ is usually much smaller than $C_{MnO2}$, we may neglect it from $C_{total}$ for simplicity. By taking the first-order derivative of $C_m$ with respect to $m_{MnO2}$ as null and using eqs. (6) and (7), one can have:

$$1 + \frac{m_{CNT} + m_{MnO_2}}{m_0} = \exp\left[\frac{m_{MnO_2}}{m_0}\right] \tag{8}$$

Although analytically unsolvable, we can plot both sides of eq. (8) as functions of $m_{MnO2}$ and search for the intersection as a graphical solution (Fig. S3). For the three PCE 10% samples with slightly different $m_0$ values, smaller $m_{CNT}$ shifts the straight line (left hand side) downwards and intersects the exponential curve (right hand side) at a small value of $m_{MnO2}$. The solution is in reasonable agreement with the experimental data. The master curve from eq. (8) can, therefore, be of great help to predict the optimal $m_{MnO2}$ if $m_{CNT}$ is given.

To fully demonstrate the versatility of the optimized electrode, a 1-min-VACNT sample coated with optimal loading (~50.7 μg) of $MnO_2$ was prepared in the PCE 10% method and characterized with various approaches. From Fig. 3a, Faradaic peaks from intercalation (cathodic, around 0.3–0.5 V vs. Ag/AgCl) and deintercalation (anodic, around 0.4–0.6 V vs. Ag/AgCl) are clearly seen at 5 mV/s and tend to smear out at higher rates ($v$). The peak current ($i_p$) can be fitted against $v$ with $a$ and $b$ as fitting parameters:

$$i_p = a v^b, \tag{9}$$

where $b$ should range theoretically between 0.5 and 1, with 0.5 standing for a diffusion-controlled Faradaic current and 1 for a surface-limited capacitive current [52]. A fitted value of 0.94 for both anodic and cathodic processes indicates a mostly capacitive nature for such an electrode (Fig. 3c), also verified by nearly straight and symmetric galvanostatic charging-discharging (GCD) curves (Fig. 3b). Certain decay in capacitance can be seen with the increased rate, as shown in Fig. 3d. The highest $C_m$ achieved is 282.6 F/g at 5 mV/s and can retain a considerable value of 161.2 F/g at extremely high scanning rate of 1 V/s, or 204.4 F/g at a large current density of 10 mA/cm$^2$. The excellent property is attributed to synergy between $MnO_2$ and VACNTs, which manifests a low series resistance ($R_s$) as ~5.45 Ω from the horizontal intercept in the Nyquist plot (Fig. 3f). Compared with uncoated VACNTs (Fig. S5), the increase in $R_s$ is insignificant, even at a relatively high mass ratio between $MnO_2$ and CNT (70:30). A tiny charge-transfer resistance ($R_{ct}$) of ~0.05 Ω can also be found from the initial unfinished semicircle (Fig. 3g). This $R_{ct}$ is insignificant compared with the reported $O(1)$ Ω values of $MnO_2$/CNT composites in the literature [17,27,28,32], implying quite fast and easy $Na^+$ adsorption/intercalation by our electrode. In addition, after 2000 GCD cycles at 1 mA/cm$^2$ (~9 A/g), the sample still holds ~87% of initial capacitance at nearly unity $\eta$, proving great stability (Fig. 3e).

## 4. Conclusion

Pulsed electrodeposition of pseudocapacitive $MnO_2$ on VACNTs is established for SC performance characterization. We discovered that $MnO_2$ coating quality is vital to the SC performance and hindered diffusion of ions across the clogging layer on top of VACNTs is responsible for the drop of $C_m$ at high $m_{MnO2}$. Our PCE approach proves quite effective in alleviating the clogging behavior. Although a state-of-the-art $C_m$ at high rate has been obtained in this work, it should be pointed out that this capacitance value still falls short of an ideal one (a theoretical specific capacitance of $MnO_2$ of 1380 F/g [3]). Further improvement is still possible, should techniques such as atomic layer deposition (ALD) be there to allow for a truly conformal coating of $MnO_2$, with perhaps a larger optimal mass loading. Practically, given the excessive cost of the ALD process, our PCE method in the liquid phase may still find its place for large-scale high-rate applications. Moreover, we foresee the possibility of extending PCE to a semi-conformal coating of various materials, *e.g.*, oxides, onto VACNTs as a low-resistance platform for many other electrical and electrochemical applications.

## Acknowledgment

We appreciate the support from Binnig and Rohrer Nanotechnology Center of ETH Zürich and IBM Zürich. We thank the NRP 70 Program “Energy Turnaround” (407040_153978) and Sinergia Programme (CRSII2-147615/1) of the Swiss National Science Foundation for financial support. We also acknowledge the SCCER Heat & Electricity Storage in collaboration with the CTI Energy Programme for provision of forum for discussion.

## Appendix A. Supplementary data

Supplementary data to this article can be found online at https://doi.org/10.1016/j.electacta.2018.11.062.

## References

[1] P. Simon, Y. Gogotsi, B. Dunn, Where do batteries end and supercapacitors begin? Science 343 (2014) 1210–1211.
[2] G. Wang, L. Zhang, J. Zhang, A review of electrode materials for electrochemical supercapacitors, Chem. Soc. Rev. 41 (2012) 797–828.
[3] D. Bélanger, L. Brousse, J.W. Long, Manganese oxides: battery materials make the leap to electrochemical capacitors, Electrochem. Soc. Interface 17 (2008) 49–52.
[4] W. Wei, X. Cui, W. Chen, D.G. Ivey, Manganese oxide-based materials as electrochemical supercapacitor electrodes, Chem. Soc. Rev. 40 (2011) 1697–1721.
[5] T.M. Higgins, D. McAteer, J.C.M. Coelho, B.M. Sanchez, Z. Gholamvand, G. Moriarty, N. McEvoy, N.C. Berner, G.S. Duesberg, V. Nicolosi, Effect of percolation on the capacitance of supercapacitor electrodes prepared from composites of manganese dioxide nanoplatelets and carbon nanotubes, ACS Nano 8 (2014) 9567–9579.
[6] X. Lang, A. Hirata, T. Fujita, M. Chen, Nanoporous metal/oxide hybrid electrodes for electrochemical supercapacitors, Nat. Nanotechnol. 6 (2011) 232–236.
[7] V. Khomenko, E. Raymundo-Pinero, F. Béguin, Optimisation of an asymmetric manganese oxide/activated carbon capacitor working at 2V in aqueous medium, J. Power Sources 153 (2006) 183–190.
[8] Y.-H. Liu, H.-C. Hsi, K.-C. Li, C.-H. Hou, Electrodeposited manganese dioxide/activated carbon composite as a high-performance electrode material for capacitive deionization, ACS Sustain. Chem. Eng. 4 (2016) 4762–4770.
[9] M. Li, H.G. Park, Pseudocapacitive coating for effective capacitive deionization, ACS Appl. Mater. Interfaces 10 (2018) 2442–2450.

[10] G. Yu, L. Hu, N. Liu, H. Wang, M. Vosgueritchian, Y. Yang, Y. Cui, Z. Bao, Enhancing the supercapacitor performance of graphene/$MnO_2$ nanostructured electrodes by conductive wrapping, Nano Lett. 11 (2011) 4438–4442.
[11] J. Yan, Z. Fan, T. Wei, W. Qian, M. Zhang, F. Wei, Fast and reversible surface redox reaction of graphene–$MnO_2$ composites as supercapacitor electrodes, Carbon 48 (2010) 3825–3833.
[12] A.G. El-Deen, N.A. Barakat, H.Y. Kim, Graphene wrapped MnO2-nanostructures as effective and stable electrode materials for capacitive deionization desalination technology, Desalination 344 (2014) 289–298.
[13] R. Rakhi, W. Chen, D. Cha, H.N. Alshareef, High performance supercapacitors using metal oxide anchored graphene nanosheet electrodes, J. Mater. Chem. 21 (2011) 16197–16204.
[14] K.-W. Nam, C.-W. Lee, X.-Q. Yang, B.W. Cho, W.-S. Yoon, K.-B. Kim, Electrodeposited manganese oxides on three-dimensional carbon nanotube substrate: supercapacitive behaviour in aqueous and organic electrolytes, J. Power Sources 188 (2009) 323–331.
[15] Y. Wang, H. Liu, X. Sun, I. Zhitomirsky, Manganese dioxide–carbon nanotube nanocomposites for electrodes of electrochemical supercapacitors, Scripta Mater. 61 (2009) 1079–1082.
[16] L. Hu, W. Chen, X. Xie, N. Liu, Y. Yang, H. Wu, Y. Yao, M. Pasta, H.N. Alshareef, Y. Cui, Symmetrical $MnO_2$–carbon nanotube–textile nanostructures for wearable pseudocapacitors with high mass loading, ACS Nano 5 (2011) 8904–8913.
[17] Y. Zhou, B. He, F. Zhang, H. Li, Hydrous manganese oxide/carbon nanotube composite electrodes for electrochemical capacitors, J. Solid State Electrochem. 8 (2004) 482–487.
[18] C. Choi, H.J. Sim, G.M. Spinks, X. Lepró, R.H. Baughman, S.J. Kim, Elastomeric and dynamic $MnO_2$/CNT core–shell structure coiled yarn supercapacitor, Adv. Energy Mater. 6 (2016) 1502119.
[19] Y. Jin, H. Chen, M. Chen, N. Liu, Q. Li, Graphene-patched CNT/$MnO_2$ nanocomposite papers for the electrode of high-performance flexible asymmetric supercapacitors, ACS Appl. Mater. Interfaces 5 (2013) 3408–3416.
[20] H. Zhang, G. Cao, Z. Wang, Y. Yang, Z. Shi, Z. Gu, Growth of manganese oxide nanoflowers on vertically-aligned carbon nanotube arrays for high-rate electrochemical capacitive energy storage, Nano Lett. 8 (2008) 2664–2668.
[21] Z. Fan, J. Chen, B. Zhang, B. Liu, X. Zhong, Y. Kuang, High dispersion of γ-$MnO_2$ on well-aligned carbon nanotube arrays and its application in supercapacitors, Diam. Relat. Mater. 17 (2008) 1943–1948.
[22] S.-B. Yoon, J.-P. Jegal, K.C. Roh, K.-B. Kim, Electrochemical impedance spectroscopic investigation of sodium ion diffusion in $MnO_2$ using a constant phase element active in desired frequency ranges, J. Electrochem. Soc. 161 (2014) H207–H213.
[23] R. Amade, E. Jover, B. Caglar, T. Mutlu, E. Bertran, Optimization of $MnO_2$/vertically aligned carbon nanotube composite for supercapacitor application, J. Power Sources 196 (2011) 5779–5783.
[24] M. Schneider, M. Weiser, C. Schrötke, F. Meißner, I. Endler, A. Michaelis, Pulse plating of manganese oxide nanoparticles on aligned MWCNT, Surf. Eng. 31 (2015) 214–220.
[25] X. Li, B. Wei, Facile synthesis and super capacitive behavior of SWNT/$MnO_2$ hybrid films, Nano Energy 1 (2012) 479–487.
[26] Y. Hou, Y. Cheng, T. Hobson, J. Liu, Design and synthesis of hierarchical $MnO_2$ nanospheres/carbon nanotubes/conducting polymer ternary composite for high performance electrochemical electrodes, Nano Lett. 10 (2010) 2727–2733.
[27] J.M. Ko, K.M. Kim, Electrochemical properties of $MnO_2$/activated carbon nanotube composite as an electrode material for supercapacitor, Mater. Chem. Phys. 114 (2009) 837–841.
[28] K. Wang, S. Gao, Z. Du, A. Yuan, W. Lu, L. Chen, $MnO_2$-Carbon nanotube composite for high-areal-density supercapacitors with high rate performance, J. Power Sources 305 (2016) 30–36.
[29] M. Narubayashi, Z. Chen, K. Hasegawa, S. Noda, 50–100 μm-thick pseudocapacitive electrodes of $MnO_2$ nanoparticles uniformly electrodeposited in carbon nanotube papers, RSC Adv. 6 (2016) 41496–41505.
[30] R. Chen, R. Poon, R.P. Sahu, I.K. Puri, I. Zhitomirsky, $MnO_2$-Carbon nanotube electrodes for supercapacitors with high active mass loadings, J. Electrochem. Soc. 164 (2017) A1673–A1678.
[31] R. Poon, I. Zhitomirsky, Supercapacitor electrodes with high active mass loading, MRS Commun. (2018) 1–4.
[32] L. Li, Z.A. Hu, N. An, Y.Y. Yang, Z.M. Li, H.Y. Wu, Facile synthesis of $MnO_2$/CNTs composite for supercapacitor electrodes with long cycle stability, J. Phys. Chem. C 118 (2014) 22865–22872.
[33] J. Yan, Z. Fan, T. Wei, J. Cheng, B. Shao, K. Wang, L. Song, M. Zhang, Carbon nanotube/$MnO_2$ composites synthesized by microwave-assisted method for supercapacitors with high power and energy densities, J. Power Sources 194 (2009) 1202–1207.
[34] P. Simon, Y. Gogotsi, Materials for electrochemical capacitors, Nat. Mater. 7 (2008) 845–854.
[35] S. Masahito, Y. Kashiwagi, Y. Li, K. Arstila, O. Richard, D.J. Cott, M. Heyns, S. De Gendt, G. Groeseneken, P.M. Vereecken, Measuring the electrical resistivity and contact resistance of vertical carbon nanotube bundles for application as interconnects, Nanotechnology 22 (2011), 085302.
[36] O. Pitkänen, T. Järvinen, H. Cheng, G. Lorite, A. Dombovari, L. Rieppo, S. Talapatra, H. Duong, G. Tóth, K.L. Juhász, On-chip integrated vertically aligned carbon nanotube based super-and pseudocapacitors, Sci. Rep. 7 (2017) 16594.
[37] M.J. Young, A.M. Holder, S.M. George, C.B. Musgrave, Charge storage in cation incorporated α-$MnO_2$, Chem. Mater. 27 (2015) 1172–1180.
[38] P. Liu, Q. Sun, F. Zhu, K. Liu, K. Jiang, L. Liu, Q. Li, S. Fan, Measuring the work function of carbon nanotubes with thermionic method, Nano Lett. 8 (2008) 647–651.
[39] J. Broughton, M. Brett, Variations in $MnO_2$ electrodeposition for electrochemical capacitors, Electrochim. Acta 50 (2005) 4814–4819.
[40] M. Huang, F. Li, F. Dong, Y.X. Zhang, L.L. Zhang, $MnO_2$-based nanostructures for high-performance supercapacitors, J. Mater. Chem. A 3 (2015) 21380–21423.
[41] I. Perez, B.L. Corso, V.R. Khalap, P.G. Collins, Conformal $MnO_2$ electrodeposition onto defect-free graphitic carbons, Electrochem. Commun. 13 (2011) 590–592.
[42] B.L. Corso, I. Perez, T. Sheps, P.C. Sims, O.T. Gül, P.G. Collins, Electrochemical charge-transfer resistance in carbon nanotube composites, Nano Lett. 14 (2014) 1329–1336.
[43] M. Toupin, T. Brousse, D. Bélanger, Charge storage mechanism of $MnO_2$ electrode used in aqueous electrochemical capacitor, Chem. Mater. 16 (2004) 3184–3190.
[44] V. Subramanian, H. Zhu, R. Vajtai, P. Ajayan, B. Wei, Hydrothermal synthesis and pseudocapacitance properties of $MnO_2$ nanostructures, J. Phys. Chem. B 109 (2005) 20207–20214.
[45] M. Xu, L. Kong, W. Zhou, H. Li, Hydrothermal synthesis and pseudocapacitance properties of α-$MnO_2$ hollow spheres and hollow urchins, J. Phys. Chem. C 111 (2007) 19141–19147.
[46] T. Gao, H. Fjellvåg, P. Norby, A comparison study on Raman scattering properties of α-and β-$MnO_2$, Anal. Chim. Acta 648 (2009) 235–239.
[47] S. Devaraj, N. Munichandraiah, Effect of crystallographic structure of $MnO_2$ on its electrochemical capacitance properties, J. Phys. Chem. C 112 (2008) 4406–4417.
[48] M.S. Dresselhaus, G. Dresselhaus, R. Saito, A. Jorio, Raman spectroscopy of carbon nanotubes, Phys. Rep. 409 (2005) 47–99.
[49] S. Agrawal, M. Raghuveer, H. Li, G. Ramanath, Defect-induced electrical conductivity increase in individual multiwalled carbon nanotubes, Appl. Phys. Lett. 90 (2007), 193104.
[50] D.M. Malone, J.L. Anderson, Hindered diffusion of particles through small pores, Chem. Eng. Sci. 33 (1978) 1429–1440.
[51] F. Wang, V.V. Tarabara, Pore blocking mechanisms during early stages of membrane fouling by colloids, J. Colloid Interface Sci. 328 (2008) 464–469.
[52] J. Wang, J. Polleux, J. Lim, B. Dunn, Pseudocapacitive contributions to electrochemical energy storage in $TiO_2$ (anatase) nanoparticles, J. Phys. Chem. C 111 (2007) 14925–14931.